Hexagonal Close-Packed Sphere Phase of Conformationally Symmetric Block Copolymer

Nai-Wen Hsu, Babak Nouri, Li-Ting Chen, and Hsin-Lung Chen*

Read Online

ACCESS | 📊 Metrics & More | 📖 Article Recommendations | 🆘 Supporting Information

ABSTRACT: The self-consistent field theory (SCFT) predicted the existence of a close-packed sphere phase over a narrow window in the phase diagram of a block copolymer (bcp). It however remains unclear whether the face-centered cubic (FCC) or hexagonal close-packed (HCP) lattice represents the more stable close-packed lattice of the spherical micelles formed by the neat bcp in the quiescent melt. Here, we revisited this problem by exploring the stable close-packed lattice of conformationally symmetric poly(ethylene oxide)-*block*-poly(1,2-butadiene) (PEO-*b*-PB). We disclosed that an HCP structure eventually formed in the ordered phase upon cooling from the micellar liquid phase. The micelle ordering was found to follow the Ostwald's step rule of the Alexander−McTague type, where a metastable BCC phase first developed followed by a transformation into the stable HCP structure. The higher thermodynamic stability of HCP relative to that of FCC was consistent with the prediction of a later SCFT calculation by Matsen and also demonstrated the generic difference between soft colloids and hard colloids in selecting their stable close-packed lattices.
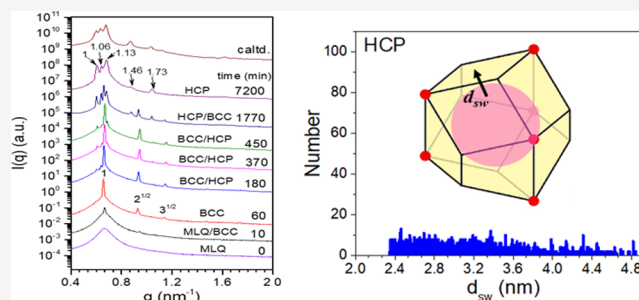
INTRODUCTION

Crystallization is the most common self-assembly process where the disordered liquid phase transforms into the crystalline phase in which the building blocks pack in the periodic lattices falling within the 230 space groups or the aperiodic quasicrystalline order. The building blocks capable of crystallizing can go beyond atoms or molecules to cover mesoscopic colloidal particles. Despite a size difference of three to four orders of magnitude, the crystallization of spherical colloidal particles and metal atoms shows strikingly similar features, particularly in their packing habit in the crystal lattice and the phase transition pathway. Body-centered cubic (BCC), face-centered cubic (FCC), and hexagonal close-packed (HCP) lattices, each comprising a single type of Voronoi cell, are the canonical packing structures of systems constituted of equivalent spheres with a nearly identical size, such as metals of a single element and colloidal particles with a narrow size distribution. FCC and HCP represent the close-packed lattices with the space groups of $Fm3m$ and $P6_3/mmc$, respectively. They are both constructed by the close stacking of two-dimensional hexagonal close-packed layers (HCPLs) of spheres but in different stacking sequences of ABCABC.. and ABABAB.. in FCC and HCP phases, respectively.[1]

A system composed of inequivalent spheres with multiplicity in particle size, such as the metallic alloy of multiple elements[2,3] and the mixture of particles of different sizes,[4] may show packing in a quasicrystalline order or the Frank−Kasper (FK) phase. The FK phase represents the tetrahedral close packing of spheres of different sizes; its characteristic

symmetry still belongs to the known space groups, but each type of lattice can be decomposed into multiple Voronoi cells with 12, 13, 15, or 16 faces (denoted as Z12, Z14, Z15, and Z16).[5]

Crystallizable colloidal particles can be categorized into hard and soft colloids. Hard colloids are spherical particles with their size and shape remaining essentially unperturbed during crystallization. They are usually inorganic nanoparticles or polymer particles with glass transition temperatures situated well above the temperature of crystallization. FCC was predicted to be the stable packing lattice for the equivalent hard spheres, with its positional entropy per sphere being only an order of 10^{-3} k_B higher than that of HCP.[6−8] Because this free energy difference is extremely small, hard colloids often crystallize to form a metastable "random hexagonal close packed (r-HCP) phase" in which the HCPLs stack in random sequences (e.g., ABACBACBA...).[9−13] The r-HCP phase could transform into a stable FCC structure slowly upon aging.[14,15]

Spherical micelles assembled using an amphiphilic surfactant or a block copolymer (denoted as "bcp" hereafter) are the representative soft colloid systems. These particles are highly
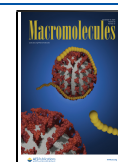
deformable and can adjust their size or even size distribution via redistributing their association numbers to fill the space homogeneously via packing in a lattice with minimum free energy. Bcp micelles can be formed in the solvent-free state (i.e., the melt state of neat bcp) or in the solution with a selective solvent, which is either a foreign solvent or the corresponding homopolymer of the constituent block. The spherical micelle formed by neat bcp consists of a core and a corona comprising the minority block and the longer majority block, respectively; the coronal region is swollen by the selective solvent in the mixture system.

An obvious deviation of the bcp micelle from the hard colloid is that the coronal blocks in the corona must fill the matrix phase homogeneously with normal segmental density; this space-filling and melt incompressibility condition perturbs the equilibrium micelle geometry from a sphere in the native form to a polyhedron in the melt state, with the polyhedral geometry determined by the packing lattice.[16,17] The lattice with the Voronoi cell showing the least deviation from the spherical geometry is usually favored.[17−21] Since the truncated octahedron cell of the BCC lattice has a higher sphericity than the rhombic dodecahedron cells of FCC and HCP, bcp micelles have been found to pack predominantly in the BCC lattice. Nevertheless, studies over the past few decades have revealed the FK phase as the more stable packing structure in a number of bcp systems, showing that even a single-component bcp may allocate the association number to the micelles according to the multiplicity of the Voronoi cell volume in a specific FK phase (e.g., σ phase).[18−28] The stability of the FK phase was attributed to the higher average sphericity of the Voronoi cells within the unit cell compared to that of the truncated octahedron of the BCC phase.[18−21] However, this type of lattice packing was displayed by bcp systems with sufficiently large asymmetry in the conformational flexibility of the constituent blocks.[19,25,26] Conformationally symmetric bcps are still prone to form equivalent micelles organized in the BCC lattice.

In addition to the BCC structure, the self-consistent field theory (SCFT) of the conformationally symmetric bcp has predicted the existence of a stable "close-packed sphere (CPS)" phase over a very narrow window in the phase diagram.[29] It is however unclear if bcp micelles in this CPS regime would still favor FCC packing over HCP, as in the case of hard colloids, considering the additional complexity arising from micelle softness and the space-filling condition. Matsen has attempted to resolve this issue through a more accurate SCFT calculation by combining the spectral method with Anderson mixing.[30] Interestingly, the result showed that HCP had a slightly lower free energy than FCC, as opposed to the hard colloid system. The difference in the calculated free energy was around 5 x $10^{-6}k_BT$ per bcp molecule;[30] considering that each bcp micelle is typically formed by several 100 molecules, the free energy difference between the HCP and FCC phases of bcp is also of the order of $10^{-3}k_BT$ per micelle.

Experimentally, although both FCC and HCP phases have been disclosed for the mixtures of bcp with foreign solvents[31,32] and the corresponding homopolymers,[33−35] to our knowledge, there were only two reports on the observation of the CPS phase in neat bcp. Imaizumi et al. reported the formation of an FCC phase in an ABA triblock copolymer, poly(1,3-cyclohexadiene)-*block*-poly(ethylene-co-but-1-ene)-*block*-poly(1,3-cyclohexadiene), after the bcp was subjected to

a flow treatment followed by thermal annealing.[36] In this case, the free energy of the copolymer was perturbed by the applied external field, so it was difficult to conclude unambiguously that FCC was more stable than HCP in the quiescent state. We have identified the coexistence of the CPS phase and the micellar liquid phase in the quiescent melt of neat poly-(ethylene oxide)-*block*-poly(1,4-butadiene) (PEO-*b*-1,4 PB).[37] The small-angle X-ray scattering (SAXS) profile of the ordered phase showed two sharp diffraction peaks with a position ratio of $1:(8/3)^{1/2}$, indicating that the micelles did not pack in the BCC lattice showing a peak position ratio of $1:2^{1/2}:3^{1/2}:..$. The ordered structure was then assigned as FCC due to the observation of this CPS phase in the blends of PEO-*b*-1,4 PB with a PB homopolymer.[33,34] However, this structure assignment suffered from ambiguity due to the absence of the $(4/3)^{1/2}$ or (200) peak, which was considered to be masked by the structure factor peak of the micellar liquid phase situated in the vicinity of the primary diffraction peak of the ordered phase. Moreover, if the stacking fault of HCPLs was taken into account, the SAXS profile was indeed analogous to that of the r-HCP phase reported recently.[35] Therefore, the assignment of FCC as the CPS phase formed in the previously studied PEO-*b*-1,4 PB was not conclusive.

Consequently, whether FCC or HCP is the more stable close-packed lattice of the spherical micelles of neat bcp in the quiescent melt remains an unsolved problem. Here, we revisit this problem by exploring the stable lattice of the CPS phase of poly(ethylene oxide)-*block*-poly(1,2-butadiene) (PEO-*b*-PB). The bcp studied here had a lower molecular weight than the one investigated previously,[37] such that the micellar liquid phase was accessed easily by moderate heating for erasing the thermal history associated with the sample preparation. The conformational asymmetry parameter ε calculated from the ratio of the Kuhn lengths of the two blocks[25,38] using $\varepsilon = (\rho_{PEO}b_{PEO}^2/\rho_{PB}b_{PB}^2)^{1/2}$ was 1.21, which was smaller than those of the conformationally asymmetric bcp systems showing FK phases.[26] Consequently, the lattice structure of the present system was not intervened by the formation of the FK phase. Using SAXS, we will disclose unambiguously that, upon cooling from the micellar liquid phase, an HCP structure was formed in the ordered phase after prolonged annealing. Moreover, a time-resolved SAXS experiment showed that the micelle ordering in the supercooled micellar liquid phase followed the Ostwald's step rule,[39] where a metastable BCC phase first developed followed by a transformation into a stable HCP structure. This finding, along with the similar ones for bcp/selective solvent mixtures unveiled by Lodge et al.,[31,32] implies the universality of the Alexander−McTague mechanism, which asserts that a BCC structure should be formed first irrespective of the stable packing lattice,[40] in soft colloid crystallization.

Finally, we will provide a detailed discussion, based principally on the theoretical works of Grason[17] and Reddy et al.,[19] on the thermodynamics of packing lattice selection of bcp micelles. We argue that, while BCC is favored for repulsive intermicellar interactions, a close-packed lattice becomes the more stable packing structure when intermicellar overlap is favored for releasing the compression of the coronal block chains if they were confined within the Voronoi cell. This scenario is encountered when the micelle size is small due to the relatively weak segregation strength.
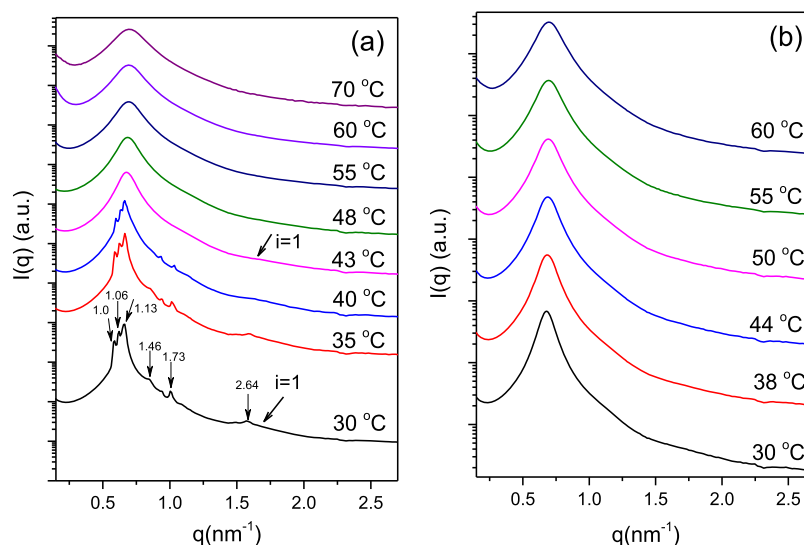
Figure 1. Temperature-dependent SAXS profiles of PEO-*b*-PB collected in (a) heating cycle and (b) subsequent cooling cycle. The SAXS profiles below 43 °C showed a series of diffraction peaks with a position ratio of 1:1.06:1.13:1.46:1.73, which was consistent with that prescribed for an ideal HCP lattice. The broad peak denoted as "*i = 1*" at ca. 1.6 nm^{-1} was the first-order form factor maximum of the microdomain formed by the PEO blocks.

■ EXPERIMENTAL SECTION

PEO-*b*-PB with the number average molecular weights (M_n) for PEO and PB blocks of 600 and 2400 g/mol, respectively, was acquired from Polymer Source, Inc. Its polydispersity index (M_w/M_n) was 1.04. The overall volume fraction of PEO (f_{PEO}) prescribed by the molecular weights of the constituents was 0.167. The sample for the SAXS experiment was prepared by solvent casting. PEO-*b*-PB was first dissolved in toluene at room temperature followed by drying in vacuo at 80 °C for 2 h to obtain the solvent-cast sample.

Temperature-dependent SAXS measurements were conducted at the beamline BL23A1 of the National Synchrotron Radiation Research Center (NSRRC), Hsinchu, Taiwan. The energy of the employed monochromatic radiation was 15 keV, with an X-ray wavelength of 0.83 Å. The 2D scattering patterns were collected with a PILATUS 1 M detector. The measured magnitude of the scattering wave vector q ranged from 0.07 to 4 nm^{-1} ($q = 4\pi/\lambda \sin(\theta/2)$, where θ is the scattering angle and λ is the wavelength). All the scattering profiles were corrected for the scatterings from air and an empty cell. The temperature ramping rate was about 5 °C/min, and the sample was allowed to equilibrate at each temperature for 5 min followed by data acquisition for 1 min.

■ RESULTS AND DISCUSSION

Formation of the HCP Phase in Neat bcp Via Ostwald's Step Rule. We utilized SAXS here to identify the packing lattice of the spherical micelles of PEO-*b*-PB. The FCC phase displays a series of diffraction peaks with a position ratio of 1:(4/3)$^{1/2}$:(8/3)$^{1/2}$:(11/3)$^{1/2}$:(12/3)$^{1/2}$, corresponding to the (111), (200), (220), (311), and (222) diffraction planes, respectively. An ideal HCP lattice with the ratio of the two lattice parameters $c/a = 1.63$ exhibits peaks with a position ratio of 1:1.06:1.13:1.46:1.73.., corresponding to the (10$\bar{1}$0), (0002), (10$\bar{1}$1), (10$\bar{1}$2), (11$\bar{2}$0).. diffractions, respectively. The peak positions follow the ratio of 1:2$^{1/2}$:3$^{1/2}$:4$^{1/2}$...associated with the (110), (200), (211), and (202) diffraction planes, respectively, for BCC packing.

We first present the SAXS results of the sample having been cooled from 80 to 27 °C followed by annealing at this temperature for 48 h to reveal the packing lattice of the spherical micelles. It is shown that 80 °C is located well above the order−disorder transition temperature (T_{ODT}) of the bcp,

such that the thermal history arising from the sample preparation was erased prior to the subsequent micelle ordering at 27 °C. It is further noted that, although the annealing temperature (27 °C) is situated below the nominal melting point of PEO (ca. 40 °C), no trace of the crystalline molecular order was found for the PEO blocks forming a micellar core or microdomain, as evidenced by the sole existence of a broad amorphous halo in the corresponding wide-angle X-ray scattering (WAXS) profile of the annealed bcp. This was due to the fact that the crystallization of PEO blocks within most spherical domains had to proceed through homogeneous nucleation, which required exceedingly large undercooling ($\Delta T > 80$ K).[41] As a consequence, the micelles assembled by the bcp molecules were considered to be liquidlike in molecular order.

Figure 1a displays the temperature-dependent SAXS profiles collected in a heating cycle of the PEO-*b*-PB sample thus treated. The SAXS profiles below 43 °C showed a series of diffraction peaks with a position ratio of 1:1.06:1.13:1.46:1.73, which was consistent with that prescribed for an ideal HCP lattice, as also demonstrated by the SAXS profile calculated using the scattering function of HCP-packed spheres developed by Förster et al., which considered the effects of finite grain size, lattice distortion, and domain size distribution for formulating the analytical expressions for the scattering functions of various lattices (see Figure 3).[42]
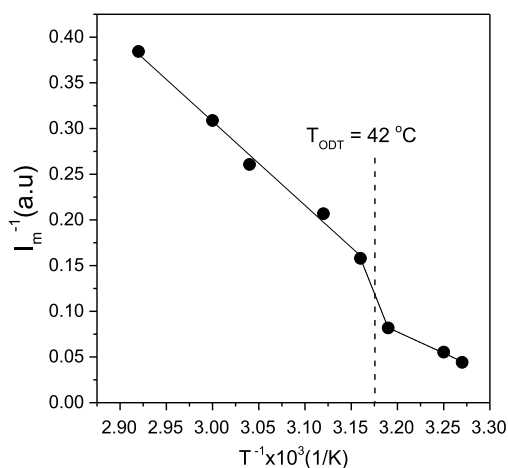
The lattice parameters deduced from the peak positions were $a = 12.3$ nm and $c = 20.0$ nm, with $c/a = 1.63$. The broad peak denoted as "*i = 1*" overlapped with a small sharp peak located at 1.57 nm^{-1}, which was the first-order form factor maximum of the micelle core or the microdomain formed by PEO blocks, as verified by the satisfactory fitting of the intensity profile in the q region of 1.1−2.4 nm^{-1} by the form factor of polydisperse spheres (see Figure S1 of the Supporting Information) assuming that the microdomain was spherical in geometry. The average radius of the spherical domain R_A deduced from the fit was 3.8 nm. The volume fraction of the microdomain calculated from the lattice parameter and R_A via

$f_{PEO} = \dfrac{\frac{4}{3}\pi\,R_A3}{\left(\frac{\sqrt{3}}{4}\right)a^2 c}$ was 0.17, which agreed well with the value of 0.167 prescribed by the block molecular weights. This close agreement indicated that there was essentially no dissociated diblock molecule or unimer in the ordered phase as the unimer had been proposed to stabilize the CPS phase in the neat bcp.[29]

The SAXS pattern turned into a broad peak at 0.7 nm^{-1} along with a shoulder at 1.2 nm^{-1} and a vague form factor maximum on heating to 43 °C. The shoulder and the form factor peak diminished progressively with further heating. The two scattering signals essentially vanished above 55 °C, where the scattering profile was only composed of a broad peak. In this case, virtually all spherical micelles dissociated in the melt, leading to a homogeneous liquid of the bcp molecules with thermal concentration fluctuations.

Figure 2 shows the plot of the inverse of the primary peak intensity (I_m^{-1}) versus the inverse of absolute temperature to
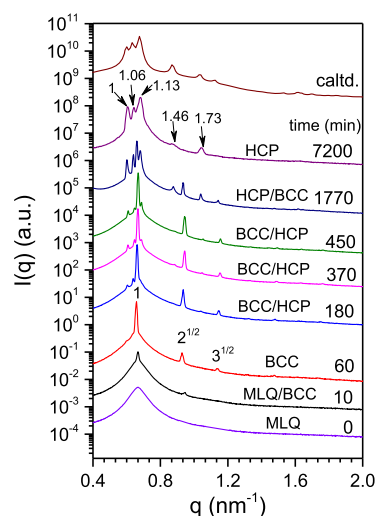

Figure 3. Time-resolved SAXS profiles of PEO-b-PB at 27 °C to resolve the micelle ordering in the supercooled micellar liquid (MLQ) phase. The sample was cooled from 80 to 27 °C followed by collecting the SAXS profiles at different annealing times. The SAXS results show that the micelle ordered into the BCC phase followed by a transformation into the HCP phase, a characteristic of the Ostwald's step rule. The SAXS profile calculated using the scattering model of the HCP lattice[42] is displayed at the top of the figure to demonstrate the close agreement between the observed SAXS profile at 7200 min and the calculated one.

Figure 2. Inverse of the primary peak intensity versus the inverse of the absolute temperature plot to identify the T_{ODT} associated with the order−disorder transition from the HCP phase to the micellar liquid phase. The T_{ODT} thus determined was 42 °C.

identify the T_{ODT} associated with the order−disorder transition from the HCP phase to the micellar liquid phase. The plot displays a weak discontinuity across the transition, indicating that the ODT was a weak first-order transition. The T_{ODT} determined from the plot was about 42 °C.

Figure 1b shows the temperature-dependent SAXS profiles collected in the subsequent cooling cycle after the bcp was heated to 70 °C. The HCP phase observed at the beginning of the heating ramp was not recovered right upon reaching 30 °C. Nevertheless, the micelles showed HCP packing after 48 h of annealing at 27 °C upon cooling from 80 °C, attesting that the ordering kinetics of the micelles was slow.

The slow kinetics allowed the micelle ordering process to be monitored by time-resolved SAXS. Here, the sample was cooled from 80 to 27 °C followed by collecting the SAXS profiles at different annealing times, as shown in Figure 3. Interestingly, two sharp peaks with a position ratio of 1:2$^{1/2}$ emerged on top of the broad halo associated with the micellar liquid phase after 10 min of annealing. These peaks grew at the expense of the broad halo, and after 60 min of annealing, a set of diffraction peaks with a position ratio of 1:2$^{1/2}$:3$^{1/2}$ were clearly identified, signifying that a BCC phase developed at the

early stage of the ordering process (see Figure S2 of the Supporting Information for detailed indexing of the diffraction peaks). Another set of peaks associated with the HCP lattice emerged clearly at 180 min, showing the later development of this close-packed structure. The HCP phase was as significant as BCC in proportion after prolonged annealing for 1770 min, and it eventually became the predominant packing lattice after 7200 min of annealing (see Figure S3 of the Supporting Information for detailed indexing of the diffraction peaks). The time-resolved SAXS results demonstrated that in the super-cooled micellar liquid, the micelles first organized into a metastable BCC phase, which subsequently transformed to a stable HCP phase. This ordering mechanism conformed to the Ostwald's step rule stipulating that the structure first developed from the supercooled liquid may not be the thermodynamically stable one, but rather the one having the free energy closer to that of the liquid phase. This metastable structure should also possess a lower activation free energy for its faster formation from the supercooled liquid.

Phenomena relevant to the Ostwald's rule have been identified for a broad spectrum of systems, ranging from atoms to colloidal particles and other soft matter, with the phase transition processes not only limited to crystallization. Proof of the Ostwald's rule requires the detailed understanding of the nucleation and growth mechanism and even the structure of the supercooled liquid. In particular, much effort has been made to resolve if there exists a universal metastable structure in the crystallization mechanism prescribed by the Ostwald's rule. On basis of the Landau theory, Alexander and McTague argued that a BCC phase should form as the metastable structure followed by a transformation into the stable lattice as long as the first-order nature of the phase transition is weak.[40] A few cases associated with the atomic crystallization of rapidly quenched metals[43,44] and the colloidal crystallization of charged hard colloids[45] and bcp micelles[31,32]

have been disclosed experimentally to develop the metastable BCC phase prescribed by the Alexander−McTague mechanism. On the other hand, studies on hard colloid crystallization have identified r-HCP as the dominant intermediate structure in the route toward the stable FCC packing;[9−13] this mechanism was also verified by the simulation works of hard-sphere colloids by Auer and Frenkel, showing that in the early stage of nucleation, r-HCP was more stable than FCC and BCC.[13] A more unified view in recent years is that BCC packing could dominate the early stage of crystallization in systems displaying Lennard−Jones and other softer potentials, while r-HCP is the dominant metastable structure in hard-sphere systems.[46]

There was no sign of the formation of the r-HCP phase in the bcp system studied here as the characteristic scattering pattern of r-HCP[35] having the same close-packed distance as that in the HCP phase was not observed throughout the micelle ordering process. Therefore, the colloidal crystallization of the spherical micelles of neat bcp toward the HCP phase was found to proceed via a BCC phase as the precursory structure. This finding, along with the similar ones for bcp/selective solvent mixtures made by Lodge et al.,[31,32] suggested the universality of the Alexander−McTague mechanism in the colloidal crystallization from the micellar liquid to the CPS phase of bcp systems.

The reason why BCC packing was favored at the initial stage of the micelle ordering was likely due to its greater similarity to the local structure of the supercooled micellar liquid, which could prescribe a lower surface free energy of the nucleus. A simulation work by ten Wolde et al.[47,48] of Lennard−Jones fluids has revealed the presence of a BCC order at the interface of a nucleus showing FCC packing at the core. This finding was later confirmed by Shen and Oxtoby, who showed a local BCC character in the equilibrium liquid−solid interface.[49] Therefore, BCC seems to be more similar to the local packing of the particles in the supercooled liquid with softer interparticle interactions. In the hard-sphere liquid, the local particle packing might show closer resemblance to a close-packed structure, such that the r-HCP phase developed predominantly in the nucleus. According to the lattice parameters deduced from Figure 3, the number densities of the micelles in HCP and BCC phases were calculated to be 7.60×10^{-4} and 8.06×10^{-4} nm^{-3}, respectively, showing that the particle number densities in the two types of lattice were slightly different. As can be seen in Figure 3, the primary scattering peak of the BCC phase and the structure factor peak of the micellar liquid were located at identical positions, whereas none of the three main diffraction peaks of the HCP phase appeared so, suggesting that BCC and the micellar liquid phase had similar local number density of micelles. As a result, the micelles first organized into BCC packing at the beginning of the ordering process in that the nucleation of the BCC phase could occur without changing the micelle number density significantly, while the formation of the HCP phase would require redistribution of the association number of the micelles to adjust into the required particle number density.

Our discussion pointed out the potential significance of the supercooled liquid structure in directing the kinetic pathway or even the eventual lattice structure of subsequent crystallization. The local structure at equilibrium is governed by the interparticle interaction; nevertheless, the long relaxation time of the micelles to reorganize into their equilibrium packing and to redistribute their association numbers in

response to the change of the surrounding condition such as temperature may lead to a nonequilibrium structure that depends strongly on its prior thermal history. Kim et al. have found that the structure of the micellar liquid of polylactide-block-polyisoprene was imprinted from the packing structure in the ordered state that it was heated from, which was either the BCC or Laves C14 phase.[23] Heating from these two ordered phases to $T > T_{ODT}$ led to micellar liquids with the structure factor peaks located at virtually the same positions as the main diffraction peaks of the corresponding ordered phases, implying that the particle number densities in the ordered state were effectively transferred into the micellar liquids. The subsequent cooling from the structured micellar liquid to $T < T_{ODT}$ recovered the original ordered phase, indicating a strong memory effect in the micellar ordering process. For the present PEO-b-PB, the copolymer was heated to 80 °C, at which the micelles had dissociated to form a uniform homogeneous liquid. In this case, the memory of the packing state in the ordered phase should have been erased, such that the perturbation from the nonequilibrium effect on the subsequent ordering process should have been circumvented.

Thermodynamic Stabilities of the Packing Lattices of bcp Micelles in the Quiescent Melt. The present study showed that HCP is favored over FCC for close packing of the spherical micelles of neat bcp. This experimental discovery verified the prediction of SCFT by Matsen showing that HCP has a slightly lower free energy than FCC.[30] It was also in parallel to our recent results revealing that the spherical micelles formed in the athermal mixtures of PEO-b-PB and the corresponding homopolymers packed into the HCP lattice upon ordering from the supercooled micellar liquid.[35] These findings attested that soft colloids behave differently from hard colloids in selecting their stable close-packed lattices as hard colloids tend to pack in the FCC lattice due to their slightly higher positional entropy.

The thermodynamics governing the lattice selection of bcp micelles becomes more complex since the spherical micelles in the native state may be deformed into the geometry of the Voronoi cells associated with the packing lattice to allow the coronal block chains to fill the matrix phase homogeneously under the melt incompressibility condition. This packing problem was first analyzed by Thomas et al.,[16] then comprehensively by Grason,[17] and recently by Reddy et al.[19] and Li et al.[24] considering micelle packing in the FK phase in the strong segregation limit.

The total free energy of the micelles with the association number N_a that packed in a lattice called "X", $F(N_a,X)$, can be decomposed into two components:

$$F(N_a, X) = F_{inter}(N_a, X) + F_{intra}(N_a, X) \qquad (1)$$

where $F_{inter}(N_a,X)$ is the free energy per micelle associated with the intermicellar interaction and $F_{intra}(N_a,X)$ is the intramicellar free energy per micelle arising from the internal structure of the micelle. These two free energy components are indeed coupled with each other. We assume that the association number of a micelle is determined by the free energy of a single micelle in its unperturbed state composed of a spherical core and a spherical shell (corona). That is, the association number is fixed first, and then the micelles seek the minimum free energy lattice for packing. Hence, the free energy components will be discussed by treating N_a as a fixed parameter.

If the intermicellar interaction is strongly repulsive, the overlap between the micellar coronas is prohibited so that each

Voronoi cell in the lattice contains a single deformed micelle. This scenario is encountered in the strong segregation regime[17,19] where the micelles formed have a large association number, leading to a small cross-sectional area per junction point. In this case, the coronal blocks are highly stretched to attain normal segmental density in the corona and would prefer to do so throughout the entire corona by themselves because overlapping with the coronas of the adjacent micelles to attain normal density requires further chain stretching to intrude into the neighboring micelles and will also cause a loss in the orientational entropy of the chain segments in the overlap region.[50]

If $F_{inter}(N_a, X)$ associated with the strong intermicellar repulsion dominates the total free energy, the micelles would seek the packing to minimize their contact area so as to minimize $F_{inter}(N_a, X)$ under the space-filling condition. Consequently, the lattice with the unit cell composed of the Voronoi cells with a minimum (average) surface area per unit volume or the highest sphericity is favored. This is the classical Kelvin problem of soap froth, which seeks the partition of space into equal volume cells with a minimum surface area. Kelvin's conjecture asserts that a truncated octahedron cell has the smallest surface area under a fixed cell volume, so the favored packing lattice is BCC.[51] Weaire and Phelan later discovered that the mean area of the Z12 and Z14 cells in the unit cell of an A15 phase under a fixed cell volume is 0.3% smaller than that of a truncated octahedron in the BCC lattice,[51] making the FK A15 phase a better candidate for space-filling packing of equivalent micelles, if the repulsive intermicellar interaction dominates their packing.

The above argument ignores the contribution of the intramicellar free energy; this may be valid for soft colloidal particles devoid of any internal structure but not for bcp micelles. A bcp micelle is composed of a core domain and a corona formed by the minority A block and the majority B block, respectively. There exists an intramicellar free energy comprising the conformational free energies of core and coronal blocks ($F_A^{conf}(N_a, X)$ and $F_B^{conf}(N_a, X)$, respectively) and the interfacial free energy ($F_\gamma(N_a, X)$) arising from the repulsion between core and coronal block chain segments in the interface, that is,

$$F_{intra}(N_a, X) = F_A^{conf}(N_a, X) + F_B^{conf}(N_a, X) + F_\gamma(N_a, X) \tag{2}$$

$F_\gamma(N_a, X)$ is minimized if the minority blocks form a spherical domain as the micellar core because sphere has the smallest surface area per unit volume. This is particularly plausible when the segregation strength is large as $F_\gamma(N_a, X) \sim \chi^{1/2}$. A spherical core is also favorable for reducing $F_A^{conf}(N_a, X)$ since the core block chains can stretch uniformly from the interface toward the center of the microdomain. Nevertheless, the stretching of the coronal blocks from the spherical domain interface to the edge of the polyhedral Voronoi cell is not uniform due to the mismatch between the curved interface of the domain and the polyhedral surface of the Voronoi cell, in particular, the chain stretching to the cell vertices can be severe.[19] As a result, formation of the spherical core domain leads to higher $F_B^{conf}(N_a, X)$. The stretching of the coronal blocks can be relaxed if the domain adopts the same shape as the Voronoi cell. This is the so-called "polyhedral-interface limit (PIL)" according to Grason, where the core−corona interface adopts a perfect, affinely shrunk copy of the shape of the Voronoi cell.[17] $F_B^{conf}(N_a, X)$ is minimized in PIL, but the

corresponding $F_\gamma(N_a, X)$ and $F_A^{conf}(N_a, X)$ are higher than those associated with the micelle comprising the spherical micro-domain.

If the bcp is conformationally symmetric, the entropy loss of A and B blocks is identical when they are subjected to the same perturbation from the unperturbed conformation. In this case, the tendency of the core block to minimize $F_A^{conf}(N_a, X)$ is offset by the tendency of the coronal block to minimize $F_B^{conf}(N_a, X)$. As a result, minimization of $F_\gamma(N_a, X)$ becomes the key factor governing the microdomain shape, which would be a sphere when χ is large. The core blocks are benefited by such an effect for uniform stretching. Then, the micelles composed of spherical domains have to seek the packing lattice that minimizes $F_B^{conf}(N_a, X)$.

Using the diblock foam model (DFM), Reddy et al. have evaluated the entropic contribution from chain stretching in a polyhedral Voronoi cell derived from the parabolic theory.[19] This model assumes that the core and coronal block chains connected by a given junction point extend along the same radial line extending from the cell center to the cell wall. The entropic contribution of chain stretching is then represented by the stretching moment governed by the average of the second-moment volumes of the Voronoi cells in the unit cell, that is,[19]

$$L(X) = \left(n_X^{-1} \sum_{i=1}^{n_X} I_i \right) / (4\pi R o^5 / 5) \tag{3}$$

where n_X is the number of Voronoi cells per unit cell, R_0 is the radius of the sphere bearing the average volume of the cells in the unit cell, and I_i is the second-moment volume of the ith cell defined as

$$I_i = \int d^3 x |x - x_i|^2 \tag{4}$$

where x_i is the center of cell i.

According to this model, a BCC lattice with a truncated octahedron cell always yields the lowest stretching moment compared with the A15 phase and other FK phases, even after the constraint of equal cell volume is relaxed.[19] Therefore, the minimum $F_{intra}(N_a, X)$ of the micelles composed of spherical core domains is attained when they pack in the BCC lattice due to the minimum entropic penalty of coronal block stretching, while the intermicellar repulsion favors packing in the A15 phase for a minimum cell area. The fact that bcp micelles predominantly pack in the BCC lattice attests that $F_{intra}(N_a, X)$ normally outweighs $F_{inter}(N_a, X)$ for the lattice selection of the conformationally symmetric bcp.

The discussion presented above was based on the premise that the intermicellar interaction is repulsive, which is encountered in the strong segregation regime. The close-packed lattices such as FCC or HCP were never found to display higher stability than the BCC or FK phase in this regime. According to the SCFT calculation, the CPS phase exists in the weak segregation regime,[17,29] where the association number and size of the micelle become small. In the unperturbed state, the micelle is composed of a spherical core with radius R_A and a coronal shell with thickness l_B, which are interrelated through

$$l_B = R_A(f_A^{-1/3} - 1) \tag{5}$$

where f_A is the volume fraction of the minority A block. It can be easily shown that l_B is smaller than the microdomain radius as long as $f_A > 0.13$, which is case of the PEO-*b*-PB studied

here (f_{PEO} = 0.167). Since the composition of the sphere-forming bcp is highly asymmetric, the chain length of the majority block is normally much longer than that of the minority block; it is hence highly probable that most coronal blocks are compressed within the corona relative to their unperturbed dimension if they are confined within the Voronoi cells under the condition of repulsive intermicellar interaction. The entropic loss per chain due to compression is given by $\Delta S \sim k_B(N_B b_B{}^2/r_B{}^2-1)$, with N_B and r_B being the number of Kuhn segments and the end-to-end distance of the compressed coronal block, respectively. To alleviate such an entropic penalty, the coronal blocks stretch out of the Voronoi cell and intrude into the coronas of the adjacent micelles, leading to an intermicellar overlap. In this case, the normal segmental density in the overlap region is attained cooperatively by the segments from the overlapping micelles. The intermicellar overlap decreases the orientational entropy of the segments in the overlap region,[50] and the micelles also lose some amount of positional entropy. These entropic losses are outweighed by the gain of conformational entropy of the coronal blocks upon releasing the chain compression.

If the overlap of a given micelle with its adjacent neighbors is favorable for attaining the normal segmental density, the micelles would seek the lattice that maximizes the overlap fraction; in this case, the Voronoi cell with the largest surface area per unit volume allows the maximum intermicellar contact and is hence favored. The cell area follows the order of FCC/HCP > BCC > A15 under a given cell volume,[17] implying that a close-packed lattice is favored for intermicellar overlap. Moreover, because each micelle in the FCC and HCP lattices is surrounded by 12 nearest neighbors with an equal distance (the nearest-neighbor distance $D_{NN} = a$ for FCC and HCP), the 12 faces of the corresponding Voronoi cells have equal area. In the case of BCC, a given micelle is surrounded by eight nearest neighbors with $D_{NN} = a$ and the other six with the longer intermicellar distance of $\frac{2}{\sqrt{3}}a$; as a result, a truncated octahedron cell has eight faces with a larger area and the other six, smaller faces. Hence, the intermicellar overlap fraction can be distributed evenly over the 12 contact faces of the Voronoi cell of close-packed lattices, whereas this is not so for BCC. A close-packed lattice is thus favored for attaining a higher overlap fraction and also for an even distribution of the overlap fraction around a given micelle.

Quantitative Characterization of the Voronoi Cells of BCC, FCC, and HCP Lattices of the PEO-*b*-PB Studied. Here, we calculated the distances from the surface of the PEO microdomain to the walls of the Voronoi cells of HCP, FCC, and BCC lattices under a given cell volume deduced from the lattice parameters of the observed HCP phase. The lattice parameters of the HCP phase formed at 30 °C by the PEO-*b*-PB were a = 12.3 nm and c = 20 nm. The volume of the primitive unit cell is $V_{uc} = 2 \times \frac{\sqrt{3}}{4} \times a^2 c = 2631.7$ nm^3. Because a primitive unit cell of the HCP lattice contains two spheres, the volume of a Voronoi cell is $V_V = V_{uc}/2 = 1315.8$ nm^3. The volume of the PEO domain in the cell is then given by $V_{PEO} = V_V f_{PEO} = 219.6$ nm^3. The Voronoi cell composed of a PEO domain the center was then constructed for the three types of lattices using the values of cell volume and domain volume.

The Voronoi cells of FCC and HCP lattices are both dodecahedrons, but their exact geometries are different due to

the different arrangements of the tetrahedral and octahedral voids. The Voronoi cell of the FCC phase is a rhombic dodecahedron with all 12 faces being parallelograms, as schematically illustrated in Figure 4a. The Voronoi cell of
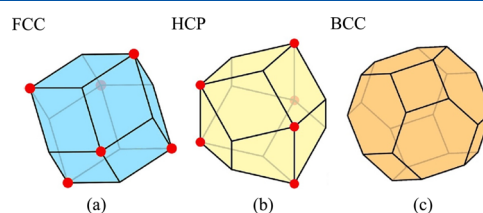
Figure 4. Schematic illustration of the Voronoi cells of (a) FCC, (b) HCP, and (c) BCC lattices. The Voronoi cell of the FCC phase is a rhombic dodecahedron with all 12 faces being parallelograms. The Voronoi cell of the HCP lattice is a trapezo-rhombic dodecahedron with six trapezoid and six parallelogram faces. The cell is a truncated octahedron for the BCC lattice. The vertices marked by red dots locate the positions of octahedron voids.

the HCP lattice is a trapezo-rhombic dodecahedron with six trapezoid and six parallelogram faces (Figure 4b). The total surface areas of the Voronoi cells calculated from the known cell volume were 649.86, 659.53, and 659.53 nm^2 for BCC, HCP, and FCC, respectively, confirming that BCC has a lower cell surface area per unit volume than the close-packed lattices.
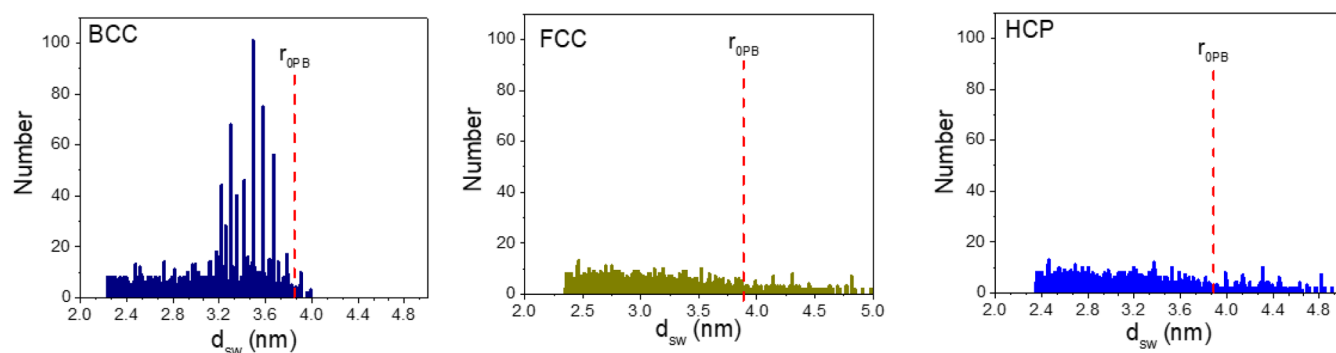
The distribution of the domain surface-to-cell wall distance (d_{sw}) was obtained by generating 10,000 lines passing through the center of the cell radially followed by locating the intersection points of these lines with the microdomain surface and the cell walls. The d_{sw} and the domain surface-to-center distance (d_{sc}) were then determined from the corresponding lengths of the lines. We considered two limiting cases for the core domain geometry, that is, the spherical domain limit (SDL) and PIL, as schematically illustrated in Figure 5.


(a) Spherical domain limit   (b) Polyhedral interface limit
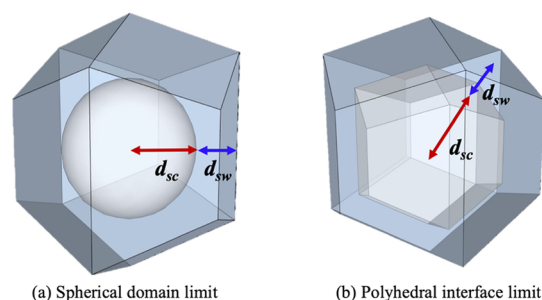
Figure 5. Two limiting cases considered for calculating the distributions of the domain surface-to-cell wall distance (d_{sw}) and the domain surface-to-center distance (d_{sc}) in the Voronoi cell: (a) spherical domain limit in which the microdomain formed in the Voronoi cell is a sphere and (b) polyhedral interface limit in which the microdomain is an affinely shrunk copy of the Voronoi cell. d_{sw} and d_{sc} were obtained by generating 10,000 lines passing through the center of the cell radially followed by locating the intersection points of these lines with the microdomain surface and the cell walls.

Figure 6 compares the distributions of d_{sw} in the three types of Voronoi cells for the two limiting cases. It is clear that PIL always generated a narrower distribution than SDL for a given type of cell. For a given type of domain geometric characteristic, the distribution of d_{sw} in the truncated octahedron cell of the BCC lattice was much narrower than those in the rhombic dodecahedron cells of FCC and HCP,

domain surface-to-cell wall distance (spherical domain limit)

domain surface-to-cell wall distance (polyhedral interface limit)
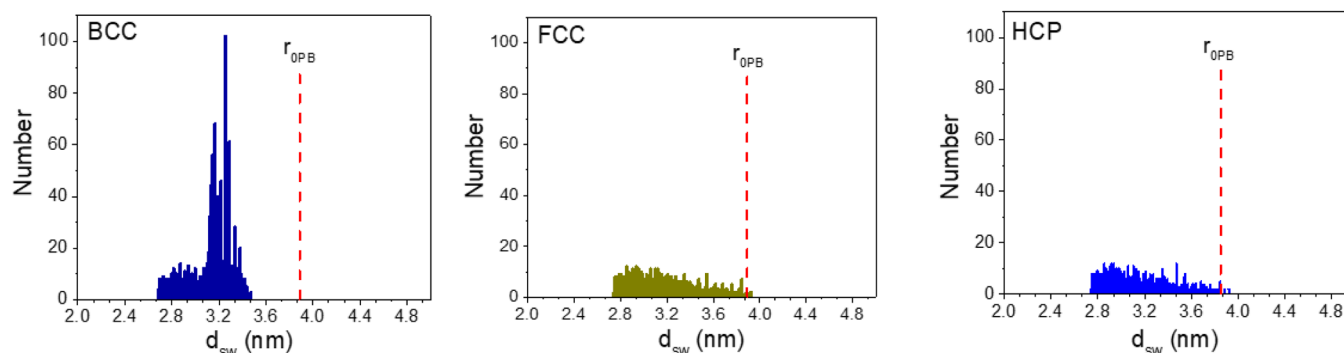
Figure 6. Distributions of d_{sw} in the three types of Voronoi cells for the two limiting cases, i.e., SDL and PIL. PIL always generates a narrower distribution than SDL for a given type of cell, and the distribution of d_{sw} in the truncated octahedron cell of the BCC lattice is much narrower than those in the rhombic dodecahedron cells of FCC and HCP for a given type of domain geometric characteristic. The distribution patterns are indistinguishable between FCC and HCP. The ranges of the abscissa and the Y axis are fixed for the three types of lattice for clear comparison of the distribution width. The vertical dashed line locates the value of the unperturbed end-to-end distance of the PB block (r_{0PB}).

and the distribution patterns were essentially indistinguishable between FCC and HCP. Figure 7 shows the distributions of d_{sw} and d_{sc} calculated by the PIL model. It is interesting to note that, for a given type of lattice, d_{sc} was in general larger than d_{sw}; the same scenario was identified for SDL, where the spherical domain radius ($R_A = 3.8$ nm) was in general larger than d_{sw}. These observations were in accord with the argument that the coronal layer thickness is smaller than the core radius once $f_A > 0.13$ in the native state of the spherical micelle.

Now we compare the calculated distances with the unperturbed end-to-end distances of PB and PEO blocks to examine if the core and coronal blocks were in general stretched or compressed if they were confined within the Voronoi cells. The unperturbed end-to-end distance is given by $r_{0i} = (C_{\infty i}N_i l_i^2)^{1/2}$ where $C_{\infty i}$, N_i, and l_i are the characteristic ratio, number of chemical bonds, and bond length of polymer i (i = PEO or PB), respectively. The values of C_∞ of PB (1,2 addition) and PEO are 7.4 and 6.9, respectively,[52] and the bond length was taken as 0.154 nm. The calculated unperturbed end-to-end distances of PB and PEO blocks were hence 3.85 and 2.56 nm, respectively. The PEO domain radius was 3.8 nm in SDL and d_{sc} was greater than 3.2 nm in PIL irrespective of the packing lattice. These values were larger than r_{0PEO} (=2.56 nm), indicating that the PEO block chains were in general stretched in the microdomain, which was consistent with the commonly predicted conformational structure of bcp. However, the values of d_{sw} were found to locate well below r_{0PB} (= 3.85 nm) over nearly the entire distribution spectrum for the BCC lattice in both the SDL and

PIL models, showing that if all the coronal block chains of a given micelle were confined within the truncated octahedron cell, they all adopted the compressed conformation. In the case of close-packed lattices composed of the spherical PEO domain, 93% of the values of d_{sw} was situated below r_{0PB}, whereas the entire spectrum was located below r_{0PB} in the PIL model, signaling that the predominant fraction of the coronal blocks should have also been compressed if they were confined within the individual Voronoi cells in both FCC and HCP phases.

The quantitative analysis of the distance distributions within the Voronoi cells thus confirmed that, while the PEO core block chains were stretched within the microdomains, most PB coronal block chains would have been compressed if they were confined within the cell under repulsive intermicellar interaction. Since chain compression was also entropically unfavorable, an effective way to release the entropic penalty was allowing the coronal blocks emanating from a given microdomain to intrude into the coronas of the adjacent micelles. The intermicellar overlap favored the close-packed lattice over BCC due to reasons discussed in the foregoing section.

Unfortunately, we were unable to identify any obvious difference in cell area and the distribution of d_{sw} between FCC and HCP; consequently, the difference in the thermodynamic stability between these two lattice structures could not be resolved straightforwardly based on the arguments provided here. Nevertheless, our experimental results showed that HCP instead of FCC eventually formed in the supercooled micellar
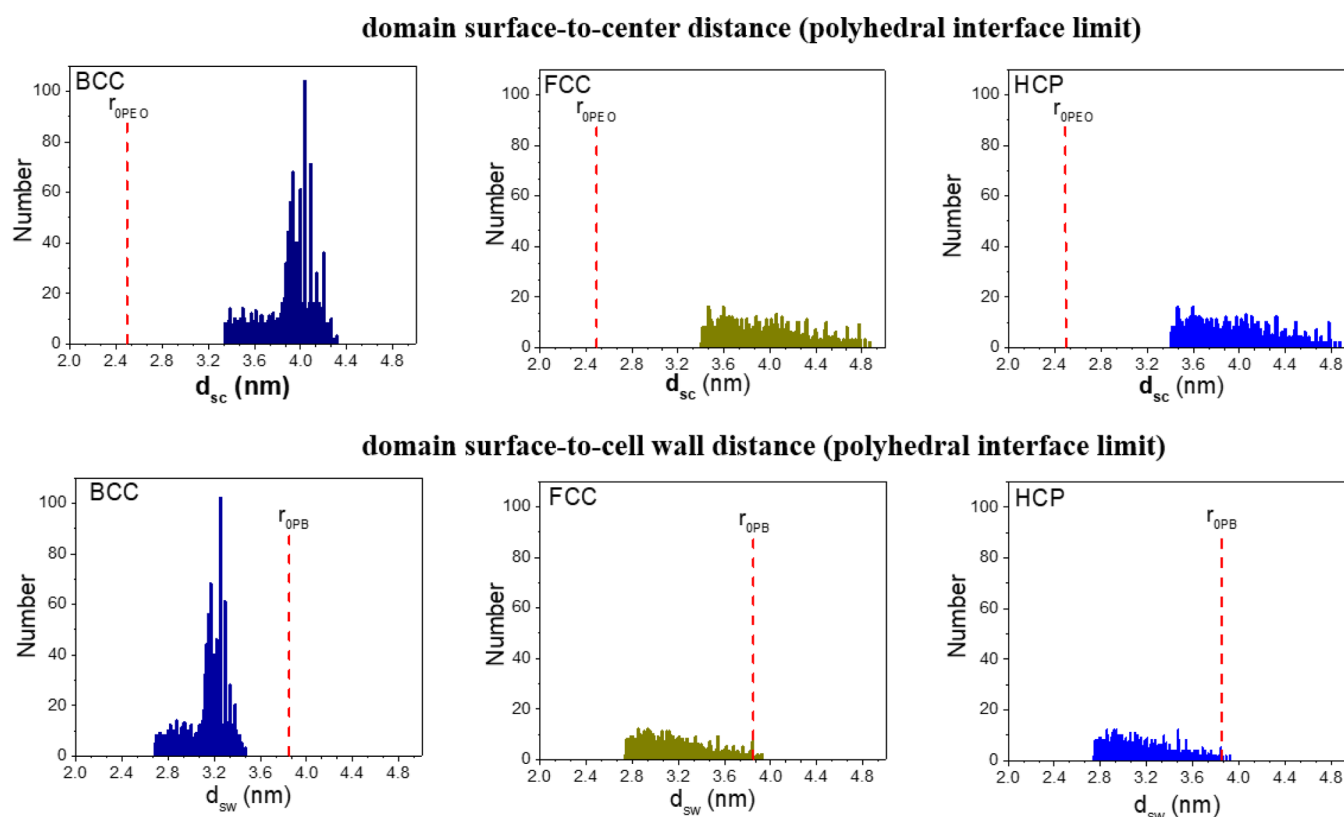
Figure 7. Distributions of d_{sw} and d_{sc} calculated by the PIL model for the three types of lattice. For a given type of lattice, d_{sc} is in general larger than d_{sw}; the same scenario is identified for SDL, where the spherical domain radius ($R_A = 3.8$ nm) is in general larger than d_{sw}. The ranges of the abscissa and the Y axis are fixed for the three types of lattice for clear comparison of the distribution width. The vertical dashed lines locate the values of the unperturbed end-to-end distances of PEO (r_{0PEO}) and PB block (r_{0PB}).

liquid phase supported by the SCFT calculation of Matsen, predicting that HCP had a slightly lower free energy than FCC under a given segregation strength.[30] However, the free energy difference was too small so that the detailed molecular mechanism associated with such a subtle difference was difficult to clarify here without sophisticated calculations of intermicellar and intramicellar free energies. Phenomenologically, our results demonstrated the intrinsic difference between hard colloids and soft colloids in selecting their close-packed lattices: hard colloids prefer FCC packing, while soft micelles favor HCP. The distinction lies in the clear difference in the underlying thermodynamic factors controlling the packing structure. Hard colloids are undeformable and devoid of an internal structure that is responsive to the particle packing structure; in this case, the positional entropy of the particles governed by the arrangement of the interstitial voids dictates the stability of the packing lattice. In the case of the bcp micelle, the free energy associated with the internal structure of the micelle is coupled with the free energy of the intermicellar interaction, and the coupling to achieve the minimum total free energy is accomplished by the responsive deformation and the overlap of the soft micelles.

CONCLUSIONS

The present study revealed that HCP is the more stable close-packed lattice than FCC for the spherical micelles formed by the neat bcp in the quiescent melt. This finding verified the SCFT prediction by Matsen that the HCP phase had a slightly lower free energy than FCC. Through analyzing the characteristics of the Voronoi cells, we found that the coronal PB blocks

would have been compressed significantly if they were confined within the cell, irrespective of whether the PEO domain was a sphere or an affinely shrunk copy of the Voronoi cell in the geometry. To release the entropic penalty arising from the chain compression, the coronal blocks extended out of the Voronoi cell and intruded into the adjacent micelles, leading to an intermicellar overlap, a different scenario from the intermicellar repulsion in the strong segregation regime that favored BCC or FK phases. In this case, the close-packed lattice was favored for attaining a higher overlap fraction and also for an even distribution of the overlap fraction around a given micelle. We further resolved the ordering mechanism of the micelles upon cooling from the micellar liquid phase and found that the process followed the Ostwald's step rule with BCC as the metastable precursor. This feature was consistent with the Alexander–McTague theory, which predicted that the BCC phase should be formed first irrespective of the stable packing lattice if the ordering process is a weak first-order transition.

ASSOCIATED CONTENT

Ⓢ Supporting Information

The Supporting Information is available free of charge at https://pubs.acs.org/doi/10.1021/acs.macromol.0c01445.

Fitting the SAXS profile collected at 30 °C in Figure 1a by the form factor of polydisperse spheres in the q region of 1.1–2.4 nm^{-1}; indexing the diffraction peaks of the PEO-b-PB sample having been annealed for 60 min at 27 °C (see Figure 3) according to the BCC lattice; and indexing the diffraction peaks of the PEO-b-PB

sample having been annealed for 7200 min at 27 °C (see Figure 3) according to the HCP lattice (PDF)

AUTHOR INFORMATION

Corresponding Author

Hsin-Lung Chen − *Department of Chemical Engineering, National Tsing Hua University, Hsinchu 30013, Taiwan;* orcid.org/0000-0002-3572-723X; Email: hlchen@che.nthu.edu.tw

Authors

Nai-Wen Hsu − *Department of Chemical Engineering, National Tsing Hua University, Hsinchu 30013, Taiwan*

Babak Nouri − *Department of Chemical Engineering, National Tsing Hua University, Hsinchu 30013, Taiwan*

Li-Ting Chen − *Department of Chemical Engineering, National Tsing Hua University, Hsinchu 30013, Taiwan*

Complete contact information is available at:
https://pubs.acs.org/10.1021/acs.macromol.0c01445

Notes

The authors declare no competing financial interest.

REFERENCES

(1) Kittel, C.; McEuen, P.; McEuen, P. *Introduction to Solid State Physics*; 8th ed.; John Wiley & Sons Inc.: New York, 1996

(2) Shoemaker, D. P.; Shoemaker, C. B. Concerning the relative numbers of atomic coordination types in tetrahedrally close packed metal structures. *Acta Crystallogr. B* **1986**, *42*, 3.

(3) Sadoc, J.F.; Mosseri, R. *Geometrical Frustration*; Cambridge University Press: Cambridge, 2000

(4) Talapin, D. V.; Shevchenko, E. V.; Bodnarchuk, M. I.; Ye, X.; Chen, J.; Murray, C. B. Quasicrystalline order in self-assembled binary nanoparticle superlattices. *Nature* **2009**, *461*, 964.

(5) Nelson, D. R.; Spaepen, F. Polytetrahedral order in condensed matter. In *Solid State Physics*, Elsevier, 1989; *42*, 1−90.

(6) Frenkel, D.; Ladd, A. J. C. New Monte Carlo method to compute the free energy of arbitrary solids. Application to the fcc and hcp phases of hard spheres. *J. Chem. Phys.* **1984**, *81*, 3188.

(7) Woodcock, L. Entropy difference between the face-centred cubic and hexagonal close-packed crystal structures. *Nature* **1997**, *385*, 141.

(8) Mau, S.-C.; Huse, D. A. Stacking entropy of hard-sphere crystals. *Phys. Rev. E* **1999**, *59*, 4396.

(9) Pusey, P. N.; Van Megen, W.; Bartlett, P.; Ackerson, B. J.; Rarity, J. G.; Underwood, S. M. Structure of crystals of hard colloidal spheres. *Phys. Rev. Lett.* **1989**, *63*, 2753.

(10) Pusey, P. N.; Van Megen, W. Phase behaviour of concentrated suspensions of nearly hard colloidal spheres. *Nature* **1986**, *320*, 340.

(11) Zhu, J.; Li, M.; Rogers, R.; Meyer, W.; Ottewill, R. H.; STS-73 Space Shuttle Crew; Russel, W. B.; Chaikin, P. M. Crystallization of hard-sphere colloids in microgravity. *Nature* **1997**, *387*, 883.

(12) Gasser, U.; Weeks, E. R.; Schofield, A.; Pusey, P.; Weitz, D. Real-space imaging of nucleation and growth in colloidal crystallization. *Science* **2001**, *292*, 258.

(13) Auer, S.; Frenkel, D. Prediction of absolute crystal-nucleation rate in hard-sphere colloids. *Nature* **2001**, *409*, 1020.

(14) Dolbnya, I. P.; Petukhov, A. V.; Aarts, D. G. A. L.; Vroege, G. J.; Lekkerkerker, H. N. W. Coexistence of rhcp and fcc phases in hard-sphere colloidal crystals. *EPL* **2005**, *72*, 962.

(15) Pronk, S.; Frenkel, D. Can stacking faults in hard-sphere crystals anneal out spontaneously? *J. Chem. Phys.* **1999**, *110*, 4589.

(16) Thomas, E. L.; Kinning, D. J.; Alward, D. B.; Henkee, C. S. Ordered packing arrangements of spherical micelles of diblock copolymers in two and three dimensions. *Macromolecules* **1987**, *20*, 2934.

(17) Grason, G. M. The packing of soft materials: Molecular asymmetry, geometric frustration and optimal lattices in block copolymer melts. *Phys. Rep.* **2006**, *433*, 1.

(18) Lee, S.; Leighton, C.; Bates, F. S. Sphericity and symmetry breaking in the formation of Frank−Kasper phases from one component materials. *PNAS* **2014**, *111*, 17723.

(19) Reddy, A.; Buckley, M. B.; Arora, A.; Bates, F. S.; Dorfman, K. D.; Grason, G. M. Stable Frank−Kasper phases of self-assembled, soft matter spheres. *PNAS* **2018**, *115*, 10233.

(20) Kim, K.; Schulze, M. W.; Arora, A.; Lewis, R. M., III; Hillmyer, M. A.; Dorfman, K. D.; Bates, F. S. Thermal processing of diblock copolymer melts mimics metallurgy. *Science* **2017**, *356*, 520.

(21) Grason, G. M.; DiDonna, B. A.; Kamien, R. D. Geometric theory of diblock copolymer phases. *Phys. Rev. Lett.* **2003**, *91*, No. 058304.

(22) Lee, S.; Bluemle, M. J.; Bates, F. S. Discovery of a Frank-Kasper σ phase in sphere-forming block copolymer melts. *Science* **2010**, *330*, 349.

(23) Kim, K.; Arora, A.; Lewis, R. M., III; Liu, M.; Li, W.; Shi, A.-C.; Dorfman, K. D.; Bates, F. S. Origins of low-symmetry phases in asymmetric diblock copolymer melts. *PNAS* **2018**, *115*, 847.

(24) Li, W.; Duan, C.; Shi, A. C. Nonclassical spherical packing phases self-assembled from AB-type block copolymers. *ACS Macro Lett.* **2017**, *6*, 1257.

(25) Xie, N.; Li, W.; Qiu, F.; Shi, A. C. σ phase formed in conformationally asymmetric AB-type block copolymers. *ACS Macro Lett.* **2014**, *3*, 906.

(26) Schulze, M. W.; Lewis, R. M., III; Lettow, J. H.; Hickey, R. J.; Gillard, T. M.; Hillmyer, M. A.; Bates, F. S. Conformational asymmetry and quasicrystal approximants in linear diblock copolymers. *Phys. Rev. Lett.* **2017**, *118*, 207801.

(27) Jeon, S.; Jun, T.; Jo, S.; Ahn, H.; Lee, S.; Lee, B.; Ryu, D. Y. Frank−Kasper Phases Identified in PDMS-b-PTFEA Copolymers with High Conformational Asymmetry. *Macromol. Rapid Commun.* **2019**, *40*, 1900259.

(28) Jayaraman, A.; Zhang, D. Y.; Dewing, B. L.; Mahanthappa, M. K. Path-dependent preparation of complex micelle packings of a hydrated diblock oligomer. *ACS Cent. Sci.* **2019**, *5*, 619.

(29) Matsen, M. W.; Bates, F. S. Unifying weak-and strong-segregation block copolymer theories. *Macromolecules* **1996**, *29*, 1091.

(30) Matsen, M. W. Fast and accurate SCFT calculations for periodic block-copolymer morphologies using the spectral method with Anderson mixing. *Eur. Phys. J. E: Soft Matter Biol. Phys.* **2009**, *30*, 361.

(31) Liu, Y.; Nie, H.; Bansil, R.; Steinhart, M.; Bang, J.; Lodge, T. P. Kinetics of disorder-to-fcc phase transition via an intermediate bcc state. *Phys. Rev. E* **2006**, *73*, No. 061803.

(32) Bang, J.; Lodge, T. P. Long-lived metastable bcc phase during ordering of micelles. *Phys. Rev. Lett.* **2004**, *93*, 245701.

(33) Huang, Y.-Y.; Chen, H.-L.; Hashimoto, T. Face-centered cubic lattice of spherical micelles in block copolymer/homopolymer blends. *Macromolecules* **2003**, *36*, 764.

(34) Huang, Y.-Y.; Hsu, J.-Y.; Chen, H.-L.; Hashimoto, T. Precursor-Driven Bcc−Fcc Order−Order Transition of Sphere-Forming Block Copolymer/Homopolymer Blend. *Macromolecules* **2007**, *40*, 3700.

(35) Chen, L.-T.; Chen, C.-Y.; Chen, H.-L. FCC or HCP: The stable close-packed lattice of crystallographically equivalent spherical micelles in block copolymer/homopolymer blend. *Polymer* **2019**, *169*, 131.

(36) Imaizumi, K.; Ono, T.; Kota, T.; Okamoto, S.; Sakurai, S. Transformation of cubic symmetry for spherical microdomains from face-centred to body-centred cubic upon uniaxial elongation in an elastomeric triblock copolymer. *J. Appl. Crystallogr.* **2003**, *36*, 976.

(37) Huang, Y.-Y.; Hsu, J.-Y.; Chen, H.-L.; Hashimoto, T. Existence of fcc-packed spherical micelles in diblock copolymer melt. *Macromolecules* **2007**, *40*, 406.

(38) Rubinstein, M.; Colby, R. H. *Polymer Physics*; Oxford University Press: Oxford, 2003.

(39) Ostwald, W. Studies on the formation and change of solid matter. *Z. Phys. Chem.* **1897**, *22*, 289.

(40) Alexander, S.; McTague, J. Should all crystals be bcc? Landau theory of solidification and crystal nucleation. *Phys. Rev. Lett.* **1978**, *41*, 702.

(41) Chen, H.-L.; Hsiao, S.-C.; Lin, T.-L.; Yamauchi, K.; Hasegawa, H.; Hashimoto, T. Microdomain-tailored crystallization kinetics of block copolymers. *Macromolecules* **2001**, *34*, 671.

(42) Förster, S.; Timmann, A.; Konrad, M.; Schellbach, C.; Meyer, A.; Funari, S. S.; Mulvaney, P.; Knott, R. Scattering curves of ordered mesoscopic materials. *J. Phys. Chem. B* **2005**, *109*, 1347.

(43) Notthoff, C.; Feuerbacher, B.; Franz, H.; Herlach, D. M.; Holland-Moritz, D. Direct determination of metastable phase diagram by synchrotron radiation experiments on undercooled metallic melts. *Phys. Rev. Lett.* **2001**, *86*, 1038.

(44) Ghosh, G. Observation and kinetic analysis of a metastable bcc phase in rapidly solidified Ni-9at.% Zr and Ni-8at.% Zr-1at.% X alloys. *Mater. Sci. Eng., A* **1994**, *189*, 277.

(45) Xu, S.; Zhou, H.; Sun, Z.; Xie, J. Formation of an fcc phase through a bcc metastable state in crystallization of charged colloidal particles. *Phys. Rev. E* **2010**, *82*, No. 010401.

(46) Tan, P.; Xu, N.; Xu, L. Visualizing kinetic pathways of homogeneous nucleation in colloidal crystallization. *Nat. Phys.* **2014**, *10*, 73.

(47) ten Wolde, P. R.; Ruiz-Montero, M. J.; Frenkel, D. Numerical evidence for bcc ordering at the surface of a critical fcc nucleus. *Phys. Rev. Lett.* **1995**, *75*, 2714.

(48) ten Wolde, P. R.; Ruiz-Montero, M. J.; Frenkel, D. Numerical calculation of the rate of crystal nucleation in a Lennard-Jones system at moderate undercooling. *J. Chem. Phys.* **1996**, *104*, 9932.

(49) Shen, Y. C.; Oxtoby, D. W. bcc symmetry in the crystal-melt interface of Lennard-Jones fluids examined through density functional theory. *Phys. Rev. Lett.* **1996**, *77*, 3585.

(50) Ziherl, P.; Kamien, R. D. Maximizing entropy by minimizing area: Towards a new principle of self-organization. *J. Phys. Chem. B* **2001**, *105*, 10147.

(51) Weaire, D.; Phelan, R. A counter-example to Kelvin's conjecture on minimal surfaces. *Philos. Mag. Lett.* **1994**, *69*, 107.

(52) Brandrup, J.; Immergut, E. H.; Grulke, E. A.; Abe, A.; Bloch, D. R. *Polymer Handbook*; 7th ed.; John Wiley & Sons Inc.: New York, 1989.